Materials Transactions, JIM, Vol. 41, No. 6 (2000) pp. 733 to 738

Formation of Ternary $L1_2$ Intermetallic Compound and Phase Relation in the Al–Ti–Fe System

Hiroshi Mabuchi, Hitoshi Nagayama*, Hiroshi Tsuda, Toshiyuki Matsui and Kenji Morii

Department of Metallurgy and Materials Science, College of Engineering, Osaka Prefecture University, Sakai 599-8531, Japan

Sintering of elemental powders and conventional arc-melting were used to form ternary $L1_2$ intermetallic compounds in the Al–Ti–Fe system. The $L1_2$ phase field and phase equilibria surrounding the $L1_2$ phase in the temperature range of interest were established. Two isothermal sections at 1423 and 1273 K were determined from metallography, X-ray diffraction and electron probe microanalyses. The compositions of $L1_2$ phase field, the center compositions of oval-shaped region, were about 28Ti–8Fe–64Al and 27Ti–9Fe–64Al compositions at 1423 and 1273 K, respectively. Thus the $L1_2$ phases had less ternary and more titanium than those reported in the other Al–Ti–X (X = Mn, Cr) systems. Besides the $L1_2$ phase, the pertinent second phases were TiAl ($L1_0$-type), $TiAl_2$ ($HfGa_2$-type), Ti_2Al_5 (28 atoms/unit cell-type), Al_3Ti ($D0_{22}$-type), C14 (Laves phase, $MgZn_2$-type), and $D8_a$ (cubic, $Mn_{23}Th_6$-type). The solubility of iron in $TiAl_2$ phase was about 2 and 3 mol% at 1423 and 1273 K, respectively. The $TiAl_2$ phase is more stable at 1273 K and can coexist with $L1_2$, TiAl, C14, and $D8_a$ phases in separate phase fields. Thus in the isothermal section at 1273 K, no two-phase equilibrium between the TiAl and $L1_2$ phases exists. This impedes the development of bonding between TiAl and $L1_2$ alloys in coating applications.

(Received February 15, 2000; Accepted May 15, 2000)

Keywords: *intermetallic compound, titanium aluminide, ternary $L1_2$ phase, phase equilibrium, aluminum-titanium-iron phase diagram*

1. Introduction

The intermetallic compound Al_3Ti is attractive as a potential high-temperature structural material because of its relatively high melting point, low density, and good oxidation resistance.[1)] However, it has the low-symmetry tetragonal $D0_{22}$ structure and is very brittle at ambient temperature. One possible approach to ductilize ordered intermetallics with low-symmetry crystal structures is to change their structures to those of higher symmetry.

The $D0_{22}$ structure of Al_3Ti can be changed to the related cubic $L1_2$ structure with the addition of a third element, such as Zn, Ni, Cu, or Fe.[2–5)] Also, many studies on the Al–Ti–X (X = Ni, Fe, Cu, Mn, Cr, Ag, and Pd *etc.*) systems have focused on the mechanical properties of the ternary $L1_2$ trialuminide compounds.[6–17)] These $(Al, X)_3Ti$ compounds will potentially have good oxidation resistance and some ductility because the $L1_2$ structure has the requisite five independent slip systems required for homogeneous deformation. The ternary $L1_2$ compounds, however, are still brittle in tension and/or bending, although they exhibit appreciable compressive ductility at ambient temperature. Recently, much work has been made on the microstructure, especially second phases and porosity generally induced by a homogenization treatment, and the microstructure-mechanical property relationships of the ternary $L1_2$ trialuminides.[18–23)] In the previous work,[24,25)] we reported that Ti–9Mn–66Al and Ti–8Cr–67Al alloys with the $L1_2$ structure posses some intrinsic bend ductility at ambient temperature, and Ti–14Mn–61Al and Ti–14Cr–61Al alloys are more ductile in bending, with a plastic strain to 0.4 and 0.9% being recorded, respectively. In these higher manganese and chromium content alloys, no porosity was observed after homogenization. The formation of porosity was caused by Kirkendall mechanism with the second phases solutionized during a homogenization treatment. Also recently, the respective bonding and coating of $L1_2$-type and $L1_0$(TiAl)-type alloys in the Al–Ti–Mn and Al–Ti–Cr systems were carried out to study functionally graded diffusion layers.[26,27)] Thus the microstructure and mechanical properties of the ternary $L1_2$ compounds are closely associated with the composition of $L1_2$ formation and equilibrium second phases surrounding the $L1_2$ phases.

In the Al–Ti–Fe system, many studies have been focused on the microstructure, mechanical properties[8,28–32)] and especially phase stability[5,33–40)] of the ternary $L1_2$ compound in Al_3Ti-base alloys. However, the phase equilibria of the Al–Ti–Fe system do not always have the same results up to now due to complexity of this system. The purpose of this work is to study the effects of iron on the formation and phase equilibrium of the ternary $L1_2$ intermetallic compound in Al_3Ti-base alloys.

2. Experimental

Specimens were prepared using two different methods. First, compound alloys were prepared by sintering of compacts made from the elemental powders; aluminum (99.9 mass%, 200 mesh), titanium (99.5 mass%, 350 mesh; containing 3500 ppm level of oxygen) and iron (99.9 mass%, 100 mesh) powders. These powders were mixed to obtain the alloy compositions, xTi–yFe–zAl (x = 25–47, y = 0–25, z = 50–75 mol%) (see later, Table 1 and Table 2). The powder mixtures, about 2 g, were pressed at about 200 MPa into a cylindrical compact of 10 mm diameter. The compacts were sintered in a tube furnace in vacuum of 1×10^{-4} Pa for 24 h/1423 K and 48 h/1273 K in order for near-equilibrium conditions to be obtained. After sintering, the samples were

*Graduate Student, Osaka Prefecture University.

blowing-air quenched from the sintering temperatures to ambient temperature. The samples were then pulverized to be a 300 mesh size. The powdered specimens were analyzed by X-ray diffraction (XRD) to identify the constituent phases in the sintered products. The X-ray radiation used was Cu K_α.

Second, using pure elemental materials (Al; 99.99 mass%, Ti; 99.7 mass%, Fe; 99.9 mass%), button ingots, approximately 30 g, with the various desired compositions (see later, Table 3) were prepared by nonconsumable electrode arc-melting under an argon atmosphere. The arc-melted buttons were remelted six times to promote chemical homogeneity. The as arc-melted alloys were annealed at 1423 K for 48 h and at 1273 K for 144 h in vacuum ($\sim 10^{-4}$ Pa) to assure the homogeneity of chemical composition and phase equilibrium, followed by blowing-air cooling. The homogenized specimens were microstructurally characterized using X-ray diffraction analysis, optical microscopy, and scanning and transmission electron microscopy (SEM and TEM). Compositions of the $L1_2$ phase and second phases were assessed by electron probe microanalysis (EPMA).

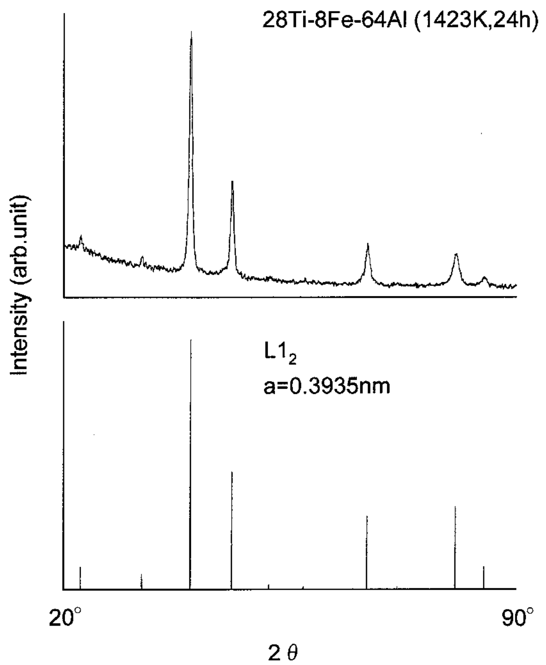

Fig. 1 XRD pattern of a sintered 28Ti–8Fe–64Al alloy and the calculated diffraction spectrum for the $L1_2$ structure.

3. Results and Discussion

3.1 Sintered alloys

The sintering process using elemental powders in the Al–Ti–X system has been discussed elsewhere.[17] Figure 1 shows the XRD pattern for a sample of sintering at 1273 K/48 h with a composition of 28Ti–8Fe–64Al. Calculated reflections and their estimated intensity for the cubic $L1_2$ structure are also shown. Thus it is confirmed that the ternary $L1_2$ intermetallic compound is formed in the Al_3Ti-base alloy containing iron. Besides the $L1_2$ phase, the pertinent phases have been also formed by the sintering of elemental powders in the binary Al–Ti and ternary Al–Ti–Fe systems. The single phases with structures, space groups and lattice parameters are given in Table 1. They are TiAl (tetragonal, $L1_0$-type), $TiAl_2$ (tetragonal, $HfGa_2$-type), Ti_2Al_5 (space group P4/mmm, 28 atoms/unit cell), Al_3Ti (tetragonal, $D0_{22}$-type), C14 (Laves phase, $MgZn_2$-type), and $D8_a$ (cubic, $Mn_{23}Th_6$-type) phases. In this work, no oxide phases were detected. However, because the exothermic synthesis process utilizes metal powders containing oxygen, the materials may contain a small volume fraction of oxide particles, *e.g.*, Al_2O_3 and TiO_2.

Of these intermetallic compound phases, $TiAl_2$ phase has been found to exist in the authors' previous work,[41] and in the studies of the $TiAl_2$-base titanium aluminides containing chromium or iron by Jewett *et al.*,[42] Durlu and Inal[43] and Yang and Goo.[37,38] The presence of Ti_2Al_5 phase has been reported by Schuster and Ipser,[44] and we have also reported[24] that the phase corresponding to the composition 28.5Ti–71.5Al is the Ti_2Al_5 phase as given in the literature.[45] The X-ray diffraction analysis as shown in Fig. 2 indicates that phase corresponding to the composition of ternary 25Ti–25Fe–50Al ($TiFeAl_2$) is the same structure as given in the studies[46–48] for the $D8_a$ phase. In the Al–Ti–X ternary systems, the $D8_a$ phase is formed when the ternary alloying element X is Fe, Co, Ni, Ru, Rh, Pd, Os, Ir and Pt, and not when that is Cr, Mn, Cu, Zn, and Ag *etc.* from Pearson's Handbook[49] of crystallographic data for intermetallic phases. The $D8_a$ phase in the Al–Ti–Fe system has been also reported by Palm *et al.*[38] as the same "τ_2" phase.

Sintered alloys of 28 different compositions were employed to determine partial phase equilibria at 1423 and 1273 K. The phases identified by XRD analysis are summarized in Table 2. Phases given in brackets are minor phases. Although the XRD analysis for a few phases is missing, the

Table 1 The single phases and lattice parameters determined by XRD analysis in the sintered alloys.

Alloy composition (powder, mol%)	Sintering condition (K, h)	Phase		Lattice parameter (nm)	
		Structure	Space group		
47Ti–53Al	1273, 48	TiAl($L1_0$)	P4/mmm	$a = 0.3995$,	$c = 0.4080$
35Ti–65Al	1273, 48	$TiAl_2$($HfGa_2$)	$I4_1$/amd	$a = 0.3971$,	$c = 2.4320$
28.5Ti–71.5Al	1423, 24	Ti_2Al_5 (28 atoms/unit cell)	P4/mmm	$a = 0.3920$,	$c = 2.9194$
25Ti–75Al	1273, 48	Al_3Ti($D0_{22}$)	I4/mmm	$a = 0.3848$,	$c = 0.8596$
28Ti–8Fe–64Al	1423, 24	$L1_2$	$Pm\bar{3}m$	$a = 0.3935$	
34Ti–20Fe–46Al	1423, 24	C14($MgZn_2$)	$P6_3$/mmc	$a = 0.5050$,	$c = 0.8200$
25Ti–25Fe–50Al	1423, 24	$D8_a$($Mn_{23}Th_6$)	$Fm\bar{3}m$	$a = 1.1990$	

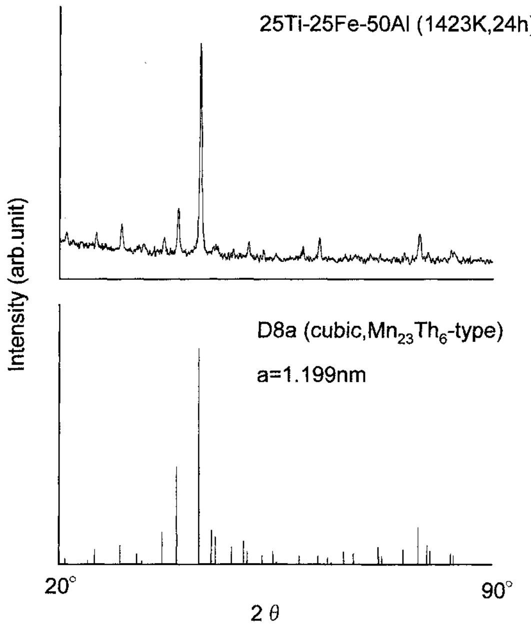

Fig. 2 XRD pattern of a sintered 25Ti–25Fe–50Al alloy and the calculated diffraction spectrum for the $D8_a$ structure.

unknown phase in brackets of the sample numbers 15 and 20 may be Ti_2Al_5 phase, which is expected to be obtained in the compositions (see later, Fig. 5). In the sample numbers 25, 26 and 28, the unknown phase in brackets will be Al_3Fe phase which does exist in the binary Al–Fe system.[50)]

3.2 Arc-melted alloys

To establish phase equilibria in the Al–Ti–Fe system, arc-melted alloys of 14 different compositions were examined metallographically and the phases and compositions were identified by XRD and EPMA analyses. The results obtained are listed in Table 3. The phases identified by XRD are similar to those in the results from the Table 1, and the chemical compositions measured by EPMA are estimated to be within the experimental error of ±0.5 mol%. The compositions of "precipitate" phases in the Table 3 did not be determined by EPMA because their microstructures were too small.

Figures 3 and 4 show SEM microstructures for two temperatures ((a) 1423 K and (b) 1273 K) of arc-melted alloys with the sample numbers 8 (33Ti–10Fe–57Al) and 11 (30Ti–14Fe–56Al), respectively. These micro-structures are two- or three-phase mixtures of $L1_2$, C14, TiAl, $TiAl_2$ or $D8_a$ phase. It is noted that a significant change of the phase equilibrium relation is observed between two temperatures. This observation suggests that these phases are transformed or decomposed by homogenization at the two different temperatures. That is, in the sample number 8, with the exception of C14 phase, the $L1_2$+TiAl (precipitate, leaf-like) two-phase region at 1423 K transforms to $TiAl_2$+$D8_a$ (precipitate, particle-like) two-phase region at 1273 K. On the other hand, in the sample number 11, the C14 and $L1_2$ phases at 1423 K transform or decompose to $TiAl_2$ and $D8_a$ phases at 1273 K, and the precipitate (striation-like) of $TiAl_2$ phase in the $L1_2$ phase is also observed. The major results from theses phase equilibria are subsequently described.

Table 2 The phases identified by XRD analysis in the sintered alloys. Phases given in brackets are minor phases.

No.	Alloy composition (powder, mol%)	Phase (s)	
		Sintered at 1423 K	Sintered at 1273 K
1	40Ti–2Fe–58Al	TiAl, (C14)	TiAl, (C14)
2	38Ti–3Fe–59Al	TiAl, C14	TiAl, C14
3	37Ti–2Fe–61Al	TiAl, ($TiAl_2$)	TiAl, ($TiAl_2$)
4	37Ti–10Fe–53Al	TiAl, C14	TiAl, C14
5	35Ti–5Fe–60Al	TiAl, $L1_2$, C14	$TiAl_2$, C14, TiAl
6	34Ti–2Fe–64Al	TiAl, ($L1_2$)	$TiAl_2$
7	34Ti–12Fe–54Al	C14, TiAl, $L1_2$	C14, $TiAl_2$
8	33Ti–3Fe–64Al	$TiAl_2$, $L1_2$	TiAl, ($L1_2$)
9	33Ti–6Fe–61Al	$L1_2$, TiAl, (C14)	$TiAl_2$, $D8_a$, ($L1_2$)
10	31Ti–4Fe–65Al	$L1_2$, $TiAl_2$	$TiAl_2$, $L1_2$
11	31Ti–6Fe–63Al	$L1_2$, (TiAl)	$TiAl_2$, $L1_2$, ($D8_a$)
12	31Ti–8Fe–61Al	$L1_2$, (C14)	$L1_2$, $TiAl_2$, $D8_a$
13	31Ti–10Fe–59Al	$L1_2$, C14	$TiAl_2$, $D8_a$, $L1_2$
14	31Ti–14Fe–55Al	$L1_2$, C14	$D8_a$, $TiAl_2$, (C14)
15	29Ti–4Fe–67Al	$L1_2$, $TiAl_2$, (?)	$L1_2$, $TiAl_2$, (?)
16	29Ti–6Fe–65Al	$L1_2$	$L1_2$, $TiAl_2$
17	29Ti–8Fe–63Al	$L1_2$	$L1_2$, $TiAl_2$
18	29Ti–10Fe–61Al	$L1_2$, (C14)	$L1_2$, $D8_a$, ($TiAl_2$)
19	29Ti–14Fe–57Al	$L1_2$, C14	$L1_2$, $D8_a$, ($TiAl_2$)
20	27Ti–4Fe–69Al	$L1_2$, Al_3Ti	$L1_2$, Al_3Ti, (?)
21	27Ti–6Fe–67Al	$L1_2$, (Al_3Ti)	$L1_2$, Al_3Ti
22	27Ti–8Fe–65Al	$L1_2$	$L1_2$, (Al_3Ti)
23	27Ti–10Fe–63Al	$L1_2$	$L1_2$, ($D8_a$)
24	27Ti–14Fe–59Al	$L1_2$, $D8_a$	$L1_2$, $D8_a$
25	25Ti–4Fe–71Al	Al_3Ti, $L1_2$, (?)	$L1_2$, Al_3Ti, (?)
26	25Ti–6Fe–69Al	$L1_2$, Al_3Ti, (?)	$L1_2$, Al_3Ti, (?)
27	25Ti–10Fe–65Al	$L1_2$, (Al_3Fe)	$L1_2$, Al_3Fe
28	25Ti–14Fe–61Al	$L1_2$, $D8_a$, (?)	$L1_2$, $D8_a$, (?)

3.3 Phase equilibria

From the above data, two isothermal sections of the equilibrium phase diagram have been experimentally determined for the Al–Ti–Fe system at 1423 and 1273 K, as shown in Figs. 5(a) and (b), respectively. These isothermal sections unambiguously show that the $L1_2$ structure is stable both at 1423 and 1273 K, and the $L1_2$ phase field at 1423 K is much larger than that at 1273 K. Thus the extent of $L1_2$ phase field increases with increasing temperature as previously pointed out by Mazdiyasni *et al.*[34)] The compositions of the $L1_2$ phase, the center compositions of oval-shaped region, are about 28Ti–8Fe–64Al and 27Ti–9Fe–64Al compositions at 1423 and 1273 K, respectively. Thus the composition of the $L1_2$ phase field is less ternary and more titanium than either reported in the Al–Ti–Mn[24)] or Al–Ti–Cr[25)] system, while it is similar to that in the Al–Ti–Ni system.[34)] The locations of the $L1_2$ phase field at two temperatures (1423 and 1273 K) are in very good agreement with the 1473 K data by Mazdiyasni *et al.*[34)] and 1273 K data by Palm and Inden.[39)]

Besides the $L1_2$ phase, two important points regarding the phase equilibria surrounding the $L1_2$ phase should be suggested to attention. First, Al_3Ti–$L1_2$ and $TiAl_2$–$L1_2$ two-phase regions are obviously observed both at 1423 and 1273 K, although the Ti_2Al_5–$L1_2$ two-phase region is not always detected, indicating that the $L1_2$ compound can be di-

Table 3 The phases and compositions identified by XRD and EPMA analyses in the arc-melted alloys.

No.	Alloy	Annealed at 1423 K				Annealed at 1423 K			
		Phase	Composition (mol%)			Phase	Composition (mol%)		
			Ti	Fe	Al		Ti	Fe	Al
1	40Ti–2Fe–58Al	TiAl	40.7	1.7	57.6				
		C14	34.6	17.8	47.6				
2	37Ti–10Fe–53Al	TiAl	38.7	2.1	59.2	TiAl	40.9	1.5	57.6
		C14	33.8	18.2	48.0	C14	34.1	18.9	47.0
3	36Ti–6Fe–58Al	TiAl	37.9	2.4	59.7	TiAl	38.6	1.6	59.8
		C14	33.8	17.2	49.0	C14	34.1	18.5	47.4
		$L1_2$	30.6	6.9	62.5	$TiAl_2$		precipitate	
4	35Ti–5Fe–60Al	TiAl	38.1	2.2	59.7	$TiAl_2$	34.3	2.2	63.5
		$L1_2$	30.0	7.4	62.6	TiAl	38.0	1.7	60.3
		C14	34.6	17.2	48.2	C14	34.0	18.6	47.4
5	35Ti–10Fe–55Al					C14	33.9	18.4	47.7
						TiAl	38.5	2.3	59.2
						$TiAl_2$		precipitate	
6	34Ti–4Fe–62Al	TiAl	37.5	2.1	60.4	$TiAl_2$	34.3	2.1	63.6
		$L1_2$	30.3	6.2	63.5	C14	32.0	19.4	48.6
		$TiAl_2$		precipitate					
7	34Ti–18Fe–48Al	C14	33.9	18.5	47.6	C14	33.6	19.1	47.3
		TiAl	40.0	2.1	57.9	$TiAl_2$	35.0	2.6	62.4
8	33Ti–10Fe–57Al	$L1_2$	30.8	7.4	61.8	$TiAl_2$	34.1	3.1	62.8
		C14	33.3	17.6	49.1	C14	34.7	17.6	47.7
		TiAl		precipitate		$D8_a$		precipitate	
9	31Ti–7Fe–62Al	$L1_2$	30.0	7.5	62.5	$L1_2$	27.4	8.5	64.1
		C14	33.2	17.6	49.2	$TiAl_2$	33.1	3.6	63.3
		TiAl		precipitate		$D8_a$	29.9	22.3	47.8
10	30Ti–5Fe–65Al	$L1_2$	29.4	6.9	63.7	$L1_2$	26.9	8.3	64.8
		$TiAl_2$	34.8	1.7	63.5	$TiAl_2$		precipitate	
11	30Ti–14Fe–56Al	$L1_2$	28.0	9.6	62.4	$D8_a$	30.3	22.7	47.0
		C14	33.3	19.4	47.3	$L1_2$	27.6	8.9	63.5
						$TiAl_2$	34.1	2.6	63.3
12	28Ti–7Fe–65Al	$L1_2$	28.1	7.1	64.8	$L1_2$	27.7	8.0	64.3
						$TiAl_2$		precipitate	
13	27Ti–14Fe–59Al	$L1_2$	26.8	10.5	62.7	$L1_2$	26.5	9.6	63.9
		$D8_a$	27.8	23.9	48.3	$D8_a$	27.6	22.8	49.6
14	25Ti–25Fe–50Al	$D8_a$	24.8	25.6	49.6	$D8_a$	24.5	25.3	50.2

rectly transformed from Al_3Ti or $TiAl_2$ compound by the addition of ternary alloying iron. Thus the stability of $L1_2$ structure may be "$TiAl_2$-base", as well as the "Al_3Ti-base", as pointed out by Durlu and Inal[43] and Yang and Goo.[38] In addition, the present data show that the solubility of iron in $TiAl_2$ phase is about 2 and 3 mol% at 1423 and 1273 K, respectively, and is larger than previously reported data by Durlu and Inal,[43] about 1 mol%. It is also noted that the decrease of temperatures leads to the increase of solubility of iron in $TiAl_2$ phase.

Second, the isothermal section at 1423 K (Fig. 5(a)) shows that the TiAl phase is in equilibrium with the $L1_2$ phase, although the width of tie line is very narrow. However, in the isothermal section at 1273 K (Fig. 5(b)), no two-phase equilibrium between the TiAl and $L1_2$ phases exists, an observation which agrees with the isothermal section at 1273 K by Palm and Inden.[39] Instead, the present study shows that the $TiAl_2$ phase is in equilibrium with the C14 and $D8_a$ phases (note that the equilibrium phase relations in the sample number 8 and 11 marked in Fig. 5 differ in two temperatures). Thus the $TiAl_2$ phase is more stable when the temperature decreases. The resulting isothermal section at 1273 K shows that the $L1_2$ phase is not in equilibrium with the TiAl phase. Therefore, in the case of Al–Ti–Fe alloys, this impedes the development of respective bonding[26] or coating[27] of TiAl and $L1_2$ alloys.

4. Conclusions

(1) In the ternary Al–Ti–Fe system, the $L1_2$ phase field

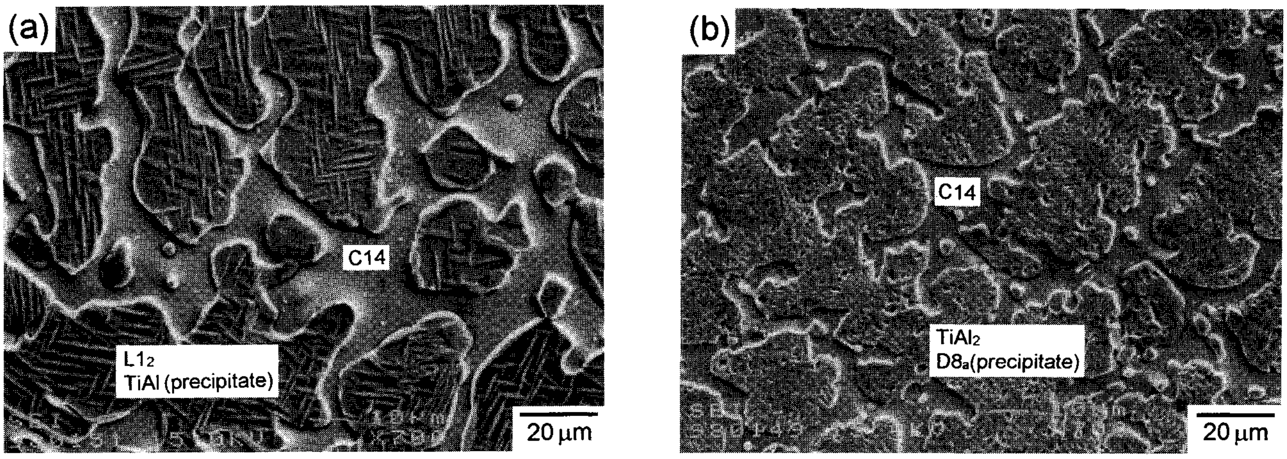

Fig. 3 SEM microstructures of sample number 8 (33Ti–10Fe–57Al) homogenized at (a) 1423 K and (b) 1273 K.

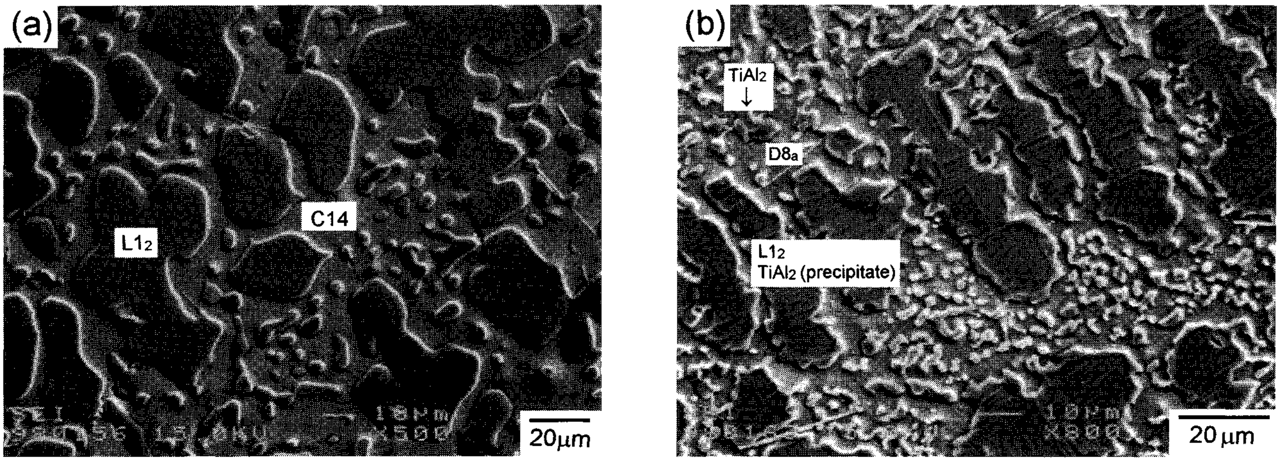

Fig. 4 SEM microstructures of sample number 11 (30Ti–14Fe–56Al) homogenized at (a) 1423 K and (b) 1273 K.

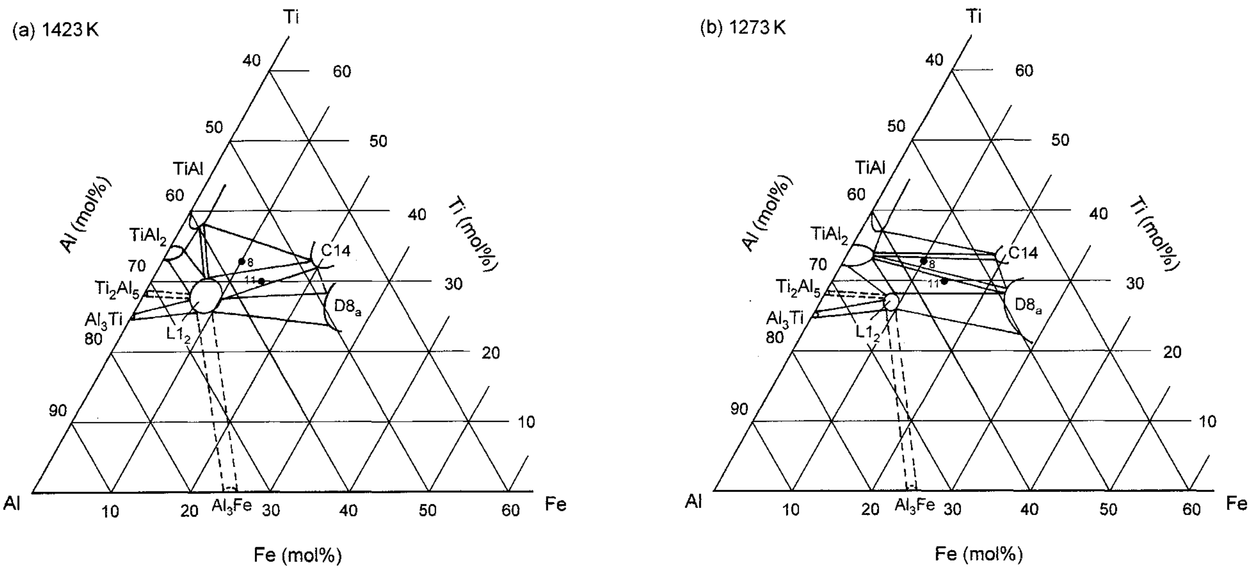

Fig. 5 The isothermal sections at (a) 1423 K and (b) 1273 K of the Al–Ti–Fe system. Solid lines are phase boundaries determined in this study. Broken lines are speculative phase boundaries. The sample numbers 8 and 11 defined in Figs. 3 and 4 are also marked on the isothermal sections.

and equilibrium second phases surrounding the $L1_2$ phase at 1423 and 1273 K have been established. These pertinent phases are TiAl, $TiAl_2$, Ti_2Al_5, Al_3Ti, C14, and $D8_a$.

(2) The $L1_2$ phase field have a poor ternary and rich titanium content compared with that reported in the other Al–Ti–X (X = Mn, Cr) systems. The center compositions of the $L1_2$ phase field are about 28Ti–8Fe–64Al and 27Ti–9Fe–64Al compositions at 1423 and 1273 K, respectively.

(3) The solubility of iron in $TiAl_2$ phase is about 2 and 3 mol% at 1423 and 1273 K, respectively, and increases when the temperature decreases. Thus the $TiAl_2$ phase is more stable at 1273 K, and is in equilibrium with $L1_2$, TiAl, C14, and $D8_a$ phases.

(4) In the isothermal section at 1273 K, no two-phase equilibrium between the TiAl and $L1_2$ phases exists. This impedes the development of respective bonding or coating of TiAl and $L1_2$ alloys.

Acknowledgments

This work was supported by a Grant-in-Aid for advanced scientific research from Osaka Prefecture University.

REFERENCES

1) M. Yamaguchi, Y. Umakoshi and T. Yamane: Phil. Mag., **55A** (1987), 301–306.
2) A. Raman and K. Schubert: Z. Metallkde., **56** (1965), 40–43.
3) A. Raman and K. Schubert: Z. Metallkde., **56** (1965), 99–104.
4) P. Virdis and U. Zwicker: Z. Metallkde., **62** (1971), 46–51.
5) A. Seibold: Z. Metallked., **72** (1981), 712–719.
6) S. C. Huang, E. L. Hall and M. F. X. Gigliotti: J. Mater. Res., **3**(1) (1988), 1–7.
7) C. D. Turner, W. O. Powers and J. A. Wert: Acta Metall., **37** (1989), 2635–2643.
8) K. S. Kumar and J. R. Pickens: Scripta Metall., **22** (1988), 1015–1018.
9) J. Tarnacki and Y.-W. Kim: Scripta Metall., **22** (1988), 329–334.
10) M. B. Winnicka and R. A. Varin: Scripta Metall., **23** (1989), 1199–1202.
11) W. E. Frazier and J. E. Benci: Scripta Matall. Mater., **25** (1991), 2267–2272.
12) H. Mabuchi, K. Hirukawa and Y. Nakayama: Scripta Metall., **23** (1989), 1761–1765.
13) S. Zhang, J. P. Nic and D. E. Mikkola: Scripta Metall. Mater., **24** (1990), 57–62.
14) H. Mabuchi, K. Hirukawa, H. Tsuda and Y. Nakayama: Scripta Metall. Mater., **24** (1990), 505–508.
15) H. Mabuchi, K. Hirukawa, K. Katayama, H. Tsuda and Y. Nakayama: Scripta Metall. Mater., **24** (1990), 1553–1558.
16) W. O. Powers and J. A. Wert: Metall. Trans., **21A** (1990), 145–151.
17) Y. Nakayama and H. Mabuchi: Intermetallics, **1** (1993), 41–48.
18) D. D. Mysko, J. B. Lumsden, W. O. Powers and J. A. Wert: Scripta Metall., **23** (1989), 1827–1830.
19) D. G. Morris and S. Gunter: Acta Metall. Mater., **40** (1992), 3065–3073.
20) J. P. Nic, J. K. Klansky and D. E. Mikkola: Mater. Sci. Eng., **A152** (1992), 132–137.
21) M. A. Winnicka and R. A. Varin: Metall. Trans., **24A** (1993), 935–946.
22) D. G. Morris and M. Leboeuf: Scripta Metall. Mater., **28** (1993), 827–832.
23) Z. L. Wu, D. P. Pope and V. Vitek: Mat. Res. Soc. Symp. Proc., **288** (1993), 367–372.
24) H. Mabuchi, A. Kito, M. Nakamoto, H. Tsuda and Y. Nakayama: Intermetallics, **4** (1996), S193–S199.
25) H. Mabuchi, H. Tsuda, T. Matsui and K. Morii: Mater. Trans., JIM, **38** (1997), 560–565.
26) H. Mabuchi, H. Tsuda, T. Tateno and K. Morii: J. Japan Inst. Metals, **62** (1998), 999–1005.
27) H. Mabuchi, H. Tsuda, T. Kawakami, S. Nakamatsu, T. Marsui and K. Morii: Scripta Mater., **41** (1999), 511–516.
28) E. P. George, W. D. Porter, H. M. Henson, W. C. Oliver and B. F. Oliver: J. Mater. Res., **4**(1) (1989), 78–84.
29) H. Gengxiang, C. Shipu, W. Xiaohua and C. Xiaofu: J. Mater. Res., **6** (1991), 957–963.
30) H. Inui, D. E. Luzzi, W. D. Porter, D. P. Pope, V. Vitek and M. Yamaguchi: Phill. Mag., **65A** (1992), 245–259.
31) D. G. Morris: Phill. Mag., **65A** (1992), 389–401.
32) Z. L. Wu and D. P. Pope: Acta Metall. Mater., **42** (1994), 509–518.
33) V. Y. Markiv, V. V. Burnashova and V. P. Ryarov: Akad. Nauk. Ukr. SSR, Metallofiz., **46** (1973), 103–110.
34) S. Mazdiyasni, D. B. Miracle, D. M. Dimiduk, M. G. Mendiratta and P. R. Subramanian: Scripta Metall., **23** (1989), 327–331.
35) K. S. Kumar: Inter. Mater. Rev., **35**(6) (1990), 293–328.
36) K. S. Kumar: *Structural Intermetallics*, ed., R. Darolia *et al.* TMS, Warrendale, PA, (1993), pp. 87–96.
37) T. Y. Yang and E. Goo: Metall. Mater. Trans., **25A** (1994), 715–721.
38) T. Y. Yang and E. Goo: Metall. Mater. Trans., **26A** (1995), 1029–1033.
39) M. Palm and G. Inden: *Structural Intermetallics*, ed., M. V. Nathal *et al.*, TMS, Warrendale, PA, (1997), pp. 73–82.
40) M. Palm, A. Gorzel, D. Letzig and G. Sauthoff: *Structural Intermetallics*, ed., M. V. Nathal *et al.*, TMS, Warrendale, PA, (1997), pp. 885–893.
41) H. Mabuchi, T. Asai and Y. Nakayama: Scripta Metall., **23** (1989), 685–689.
42) T. J. Jewett, B. Ahrens and M. Dahms: Intermetallics, **4** (1996), 543–556.
43) N. Durlu and O. T. Inal: Mater. Sci. Eng., **A152** (1992), 67–75.
44) J. C. Schuster and H. Z. Ipser: Z. Metallkde., **81** (1990), 389–396.
45) R. Miida, M. Kasahara and D. Watanabe: Jap. J. Appl. Phys., **19** (1980), L707–L710.
46) J. V. Florio, R. E. Rundie and A. I. Snow: Acta Cryst., **5** (1952), 449–457.
47) E. I. Gladyshevskii, P. I. Kripyakurich, Y. B. Kuzma and M. Y. Teslyuk: Sov. Phys. Crystallogr., **6** (1961), 615–616.
48) A. Khataee, H. M. Flower and D. R. F. West: Mater. Sci. Technol., **5** (1989), 632–643.
49) P. Villars and L. D. Calvert: *Pearson's Handbook of Crystallographic Data for Intermetallic Phases*, ASM, Metals Park, OH, (1985), Vol. 1–3.
50) T. B. Massalski: *Binary Alloy Phase Diagrams*, 2nd edn, ASM Metals Park, PH, Vol. 1 (1990), pp. 111–112.